ACS APPLIED BIO MATERIALS Cite This: ACS Appl. Bio Mater. XXXX, XXX, XXX−XXX

Article

www.acsabm.org

Reduced Graphene Oxide-Zirconium Dioxide−Thionine Nanocomposite Integrating Recognition, Amplification, and Signaling for an Electrochemical Assay of Protein Kinase Activity and Inhibitor Screening

Zhiqiang Chen,[†] Ying Liu,[†] Lijie Hao,[†] Zhencai Zhu,[‡] Fang Li,[‡] and Shufeng Liu*[,†]

[†]Key Laboratory of Optic-Electric Sensing and Analytical Chemistry for Life Science, Ministry of Education, College of Chemistry and Molecular Engineering, Qingdao University of Science and Technology, 53 Zhengzhou Road, Qingdao, Shandong 266042, China

[‡]College of Marine Science and Biological Engineering, Qingdao University of Science and Technology, 53 Zhengzhou Road, Qingdao, Shandong 266042, China

Supporting Information

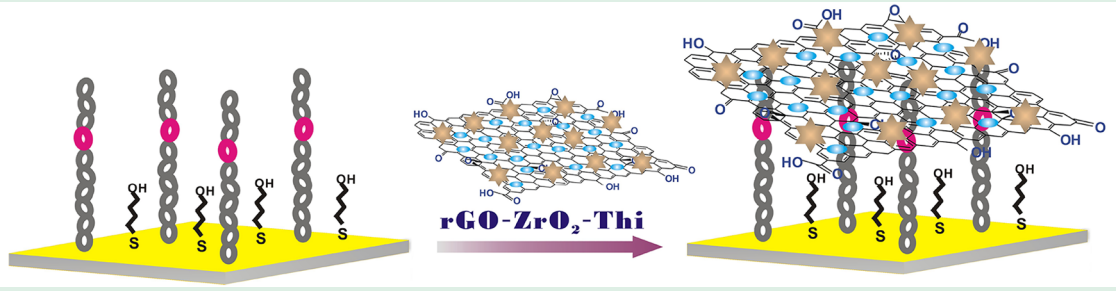

ABSTRACT: Protein kinase activity analysis is essential and important for elucidation of many fundamental biological processes, disease diagnosis, and drug discovery. Herein, a novel electrochemical biosensing method for protein kinase (PKA) activity was demonstrated by the use of a reduced graphene oxide-zirconium dioxide−thionine (rGO-ZrO_2−Thi) nanocomposite, which interestingly served as an integral phosphopeptide-recognizing, signal amplifying and reporting platform. The ZrO_2 nanoparticle-decorated reduced graphene oxide (rGO-ZrO_2) was first prepared by a hydrothermal reaction route, and then the thionine was conjugated onto the rGO surface via $\pi-\pi$ stacking as an excellent electrochemical probe. The prepared rGO-ZrO_2−Thi nanocomposites were well-characterized by various techniques. With the full advantage of specific recognition of ZrO_2 nanoparticles for the phosphate group, signal amplification, and transduction of abundant thionines onto the rGO surface, and excellent conductivity of rGO, the rGO-ZrO_2−Thi nanocomposite endowed a label-free and one-step electrochemical analysis of kemptide phosphorylation catalyzed by PKA. The detection limit for PKA activity was experimentally achieved as 0.005 U/mL, which was evidently lower than most of the reported methods. The proposed sensing strategy could be also applied for an efficient inhibitor evaluation. Therefore, it offered an excellent pathway for a generic and sensitive electrochemical assay of PKA activity and inhibitor.

KEYWORDS: *reduced graphene oxide, zirconia, protein kinase activity, electrochemical biosensor*

1. INTRODUCTION

Protein kinase (PKA) can catalyze protein phosphorylation that is involved in cellular signal transduction to regulate many essential cellular functions.[1−3] An aberrant level of PKA activity and phosphorylation state has been directly connected with many clinical diseases, for example, cancer and immune deficiency-, neurodegenerative-, and endocrinological disorder-related diseases.[4−6] Protein kinases are also widely used as therapeutic targets for drug design and discovery.[7,8] Thus, identification of PKA activity is essential and important for elucidation of signal transduction mechanisms, understanding of fundamental biological processes, disease diagnosis, and drug discovery.

During the past decades, there have been numerous reports that focus on the analysis of PKA activity by different techniques including electrochemistry, fluorescence, colorimetry, photoelectrochemistry, electrochemiluminescence, etc.[9−19] Among them, electrochemical methods show some prominent advantages, for example, intrinsic stability, simple instrumentation, operational flexibility, ease of miniaturization, and good sensitivity. The detection principle for PKA by these existing techniques can be concluded as two classes. The

Received: August 20, 2018
Accepted: October 12, 2018
Published: October 12, 2018

DOI: 10.1021/acsabm.8b00451
ACS Appl. Bio Mater. XXXX, XXX, XXX−XXX

Scheme 1. (A) Schematic Illustration of the Synthesis of the rGO-ZrO_2−Thi Nanocomposite and (B) Fabrication Principle of the Electrochemical Biosensor for the Protein Kinase Activity Assay

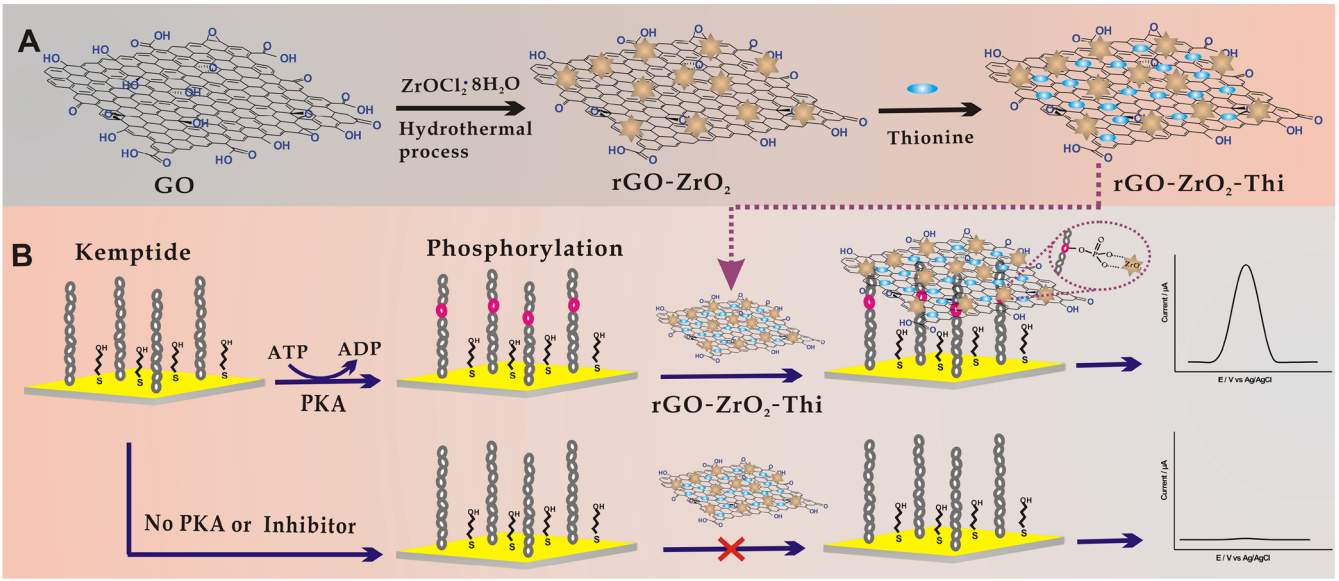

labeling technique can be regarded as a widely used type for PKA activity evaluation. In this case, the radioactive, electroactive, fluorescent, biotin, or thiol labels could be introduced into the kemptide substrate after PKA catalysis with the use of corresponding ATP analogues as alternatives and then for direct or amplified analysis of PKA.[20−25] Another type relies on the phosphorylation-specific recognition elements, for example, antibody, metal ions, metal complexes, and nanomaterials, which play a signal mediation or transition role for profiling protein kinase activity.[26−31] For example, the Liu and Li groups realized the sensitive fluorescence analysis of PKA on the basis of novel rare earth ion-functionalized microbead or Zr^{4+}-functionalized mesoporous SiO_2 microspheres.[32,33] These endeavors have made great progress for PKA analysis, but the involved labor-intensive labeling procedures or radiolabeling or specialized assay reagents increase the assay complexity and cost. Also, the detection sensitivity toward PKA needs to be further upgraded to serve better for disease diagnosis and drug discovery. Currently, Zr^{4+} has been well-employed for the enrichment of a phosphorylated peptide since its multicoordinative interaction with a phosphate group.[34,35] It has also been explored to fabricate a sensitive PKA biosensor. For example, DNA-, polymer-, or nanomaterial-based signal amplification systems have been established for the sensitive PKA assay using this Zr^{4+} multicoordination-based signal transduction method.[36−41] However, they are often plagued with the relatively complex operation procedures on the electrode. Therefore, the fabrication of an electrochemical biosensor with the advantages of simplicity, reliability, and striking sensitivity still remains a great challenge for PKA analysis.

Herein, we introduced a simple but very sensitive protocol for electrochemical monitoring of PKA activity with the use of a new reduced graphene oxide-zirconium dioxide−thionine (rGO-ZrO_2−Thi) nanocomposite as an all-in-one platform for phosphopeptide recognition, signal amplification, and readout. The ZrO_2 nanoparticle-decorated reduced graphene oxide (rGO-ZrO_2) was first prepared via a simple hydrothermal reaction process.[42−44] Then the electrochemical probe, thionine (Thi), was conjugated onto the rGO surface via $\pi-\pi$ interaction to obtain a rGO-ZrO_2−Thi nanocomposite.[45,46] As to this nanocomposite, ZrO_2 was committed to phosphopeptide recognition. Due to the unique electronic properties and large surface area of rGO, the adsorbed abundant thionine molecules on it were responsible for signal amplifying and reporting. The obtained rGO-ZrO_2−Thi nanocomposite was then used for PKA biosensor fabrication. The immobilized kemptide on the electrode could be phosphorylated by PKA and ATP and then captured by the rGO-ZrO_2−Thi nanocomposite for amplified electrochemical responses related with PKA activity.

2. EXPERIMENTAL SECTION

2.1. Reagents and Materials. Graphene oxide was directly purchased from Shanghai Tanyuanhuigu Co., Ltd. (Shanghai, China). Cysteine-terminated kemptide (LRRASLGGGGC) and ATP were obtained from Sangon Biotech Co., Ltd. (Shanghai, China). The cAMP-dependent protein kinase (PKA), exonuclease III (Exo III), and T4 polynucleotide kinase (T4 PNK) were obtained from New England Biolabs Inc. (Ipswich, MA, USA). 6-Mercapto-1-hexanol (MCH), $ZrOCl_2·8H_2O$, and thionine (Thi) were purchased from Sigma-Aldrich (St. Louis, MO, USA). Bovine serum albumin (BSA), thrombin, and fetal calf serum (FBS) were obtained from Dingguo Biotech Co., Ltd. (Beijing, China). *N*-(3-Chlorophenyl)-6,7-dimethoxy-4-quinazolinamine (Tyrphostin AG1478), ellagic acid, and *N*-[2-(*p*-bromocinnamylamino)ethyl]-5-isoquinolinesulfonamide dihydrochloride (H-89) were supplied by Aladdin Reagents Inc. (Shanghai, China).

2.2. Synthesis of the rGO-ZrO_2 Nanocomposite. The synthesis of the rGO-ZrO_2 nanocomposite was based on a simple hydrothermal reaction process.[42−44] Briefly, 0.004 g of $ZrOCl_2·8H_2O$ and 0.004 g of GO were mixed into 20 mL of deionized water, and the mixture was ultrasonically treated for 1 h. The hydrothermal reaction for the above mixture was operated at 160 °C for 10 h. Then, the precipitate was collected by centrifugation at 5000 r/min for 5 min and thoroughly washed with deionized water. After the precipitate was freeze-dried (−80 °C, 24 h), the rGO-ZrO_2 nanocomposite was obtained. The mass ratio of GO and $ZrOCl_2·8H_2O$ was changed from 1:5 to 1:0.2 for the preparation of different rGO-ZrO_2 nanocomposites.

DOI: 10.1021/acsabm.8b00451
ACS Appl. Bio Mater. XXXX, XXX, XXX−XXX

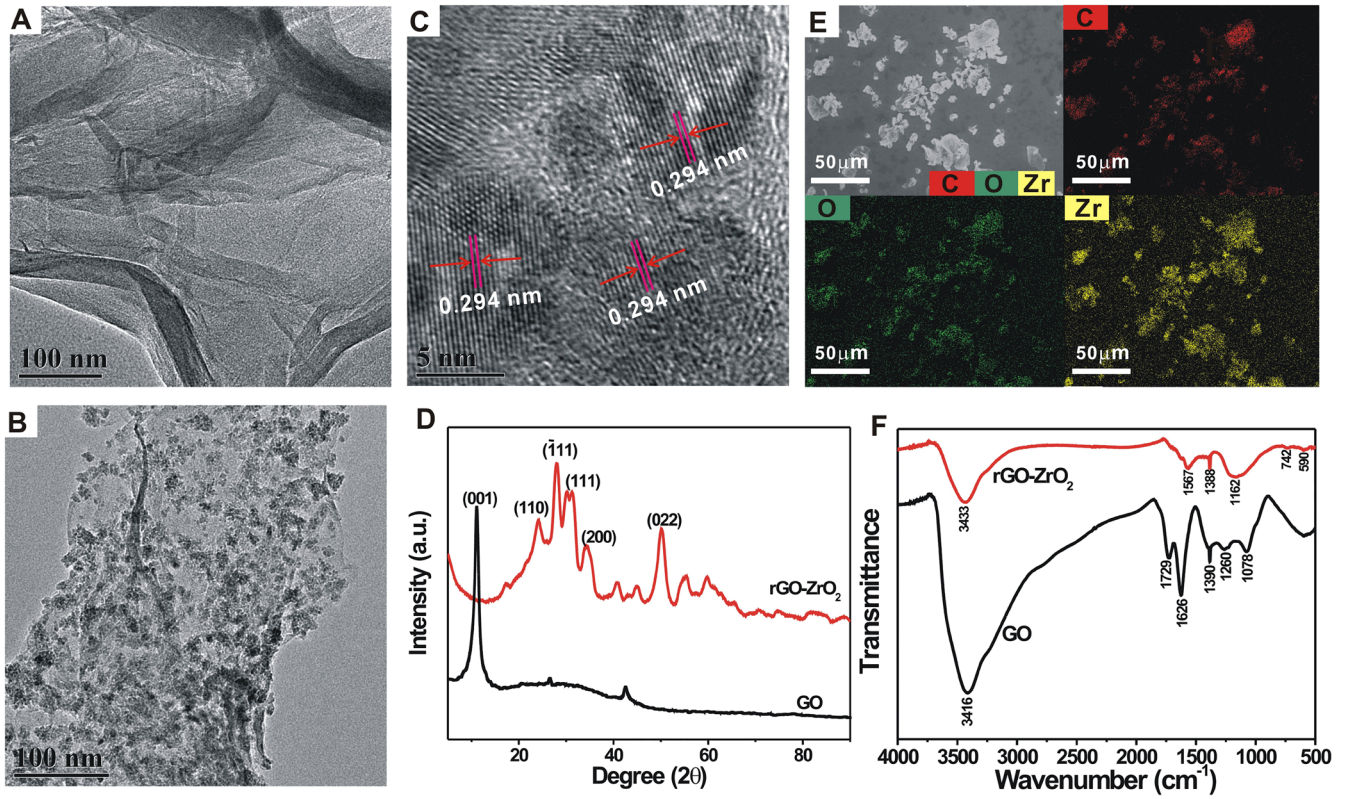

Figure 1. TEM images for GO (A) and rGO-ZrO_2 (B). (C) High-resolution TEM image of rGO-ZrO_2. (D) XRD patterns of GO and rGO-ZrO_2. (E) Corresponding elemental mapping images of C, O, and Zr. (F) FTIR spectra of GO and rGO-ZrO_2.

2.3. Assembly of Thionine on the rGO-ZrO_2 Nanocomposite. A total of 2.5 mg of rGO-ZrO_2 was added into 10 mL of thionine solution (1 mM), and the mixture was agitated ultrasonically for 1 h. After filtration through a 0.45 μm nylon filter followed by thorough washing and vacuum drying, the rGO-ZrO_2−Thi nanocomposites were prepared.

2.4. Kemptide Immobilization. The pretreatment of the gold electrode was operated according to the reported procedure.[47] The immobilization of kemptide was executed by incubating into 200 μM kemptide in 10 mM Tris-HCl buffer (pH 7.4, 0.2 M NaCl, 10 mM TCEP, 1 mM EDTA) overnight at room temperature. After being washed thoroughly with 10 mM Tris-HCl buffer (pH 7.4, 0.1 M NaCl), the kemptide-immobilized electrode was treated with 1 mM MCH for 45 min and washed with Tris-HCl buffer.

2.5. PKA-Catalyzed Kemptide Phosphorylation and Recognition by the rGO-ZrO_2−Thi Nanocomposite. The phosphorylation of the immobilized kemptide was conducted in 50 mM Tris-HCl buffer (pH 7.4, 20 mM $MgCl_2$) containing 80 μM ATP and various concentrations of PKA for 90 min at 37 °C. After being washed by Tris-HCl buffer, the phosphorylated kemptide was recognized by 0.5 mg/mL rGO-ZrO_2−Thi nanocomposite for 1 h at room temperature. Then, the electrode was directly used for electrochemical interrogation.

2.6. PKA Inhibitor Screening. The PKA inhibitor screening was performed by almost the same procedures as above except that various concentrations of inhibitor were added into the buffer.

2.7. Electrochemical Measurement. Electrochemical tests for the modified electrodes were conducted in 10 mM PBS buffer (pH 7.4) by using differential pulse voltammetry (DPV) and cyclic voltammetry (CV) techniques. DPV was scanned from 0.1 to −0.4 V with a pulse amplitude and period set at 50 mV and 0.1 s, respectively. CV was scanned in the potential range from −0.2 and 0.6 V at 50 mV/s. The electrochemical impedance spectroscopy (EIS) characterization toward the biosensor fabrication process was conducted in 5 mM $[Fe(CN)_6]^{3-/4-}$ of 10 mM PBS buffer (pH 7.4, 1 M KCl). The applied frequency was in the range from 0.1 Hz to 10 K Hz.

2.8. Apparatus. The corresponding instruments and types used for characterization of the nanocomposites and biosensor were listed in the Supporting Information.

3. RESULTS AND DISCUSSION

3.1. Preparation of the rGO-ZrO_2−Thi Nanocomposite and the Detection Principle for Protein Kinase Activity. The ZrO_2 nanoparticle-decorated reduced graphene oxide (rGO-ZrO_2) was first prepared by a facile hydrothermal reaction process using graphene oxide (GO) and $ZrOCl_2$ as reactants (Scheme 1A). The $ZrOCl_2$ precursor could be hydrolyzed into the Zr (IV) complex ions, which were then physically or chemically adsorbed onto the GO surface and transformed into ZrO_2 nanoparticles under hydrothermal conditions. Simultaneously, the GO was reduced into rGO to obtain the rGO-ZrO_2 nanocomposite.[43,48] Subsequently, the thionine (Thi) could be attached onto the bare rGO surface via $\pi-\pi$ stacking to obtain the rGO-ZrO_2−Thi nanocomposite, which served as an excellent electrochemical probe because of its high specific surface characteristic, unique electronic properties, and biocompatibility of rGO.[45,46] Then, the rGO-ZrO_2−Thi nanocomposite was explored for the one-step and label-free electrochemical analysis of kemptide phosphorylation catalyzed by PKA (Scheme 1B). The assembly of cysteine-terminated kemptide on the electrode was based on the interaction of Au with the thiol group of cysteine. The phosphorylation of immobilized kemptide was accomplished by the PKA-catalyzed transfer of the γ-phosphate group of ATP into the serine of kemptide. The phosphorylated kemptide then directly captured the rGO-ZrO_2−Thi nanocomposite by the multicoordinative interaction between ZrO_2

DOI: 10.1021/acsabm.8b00451
ACS Appl. Bio Mater. XXXX, XXX, XXX−XXX

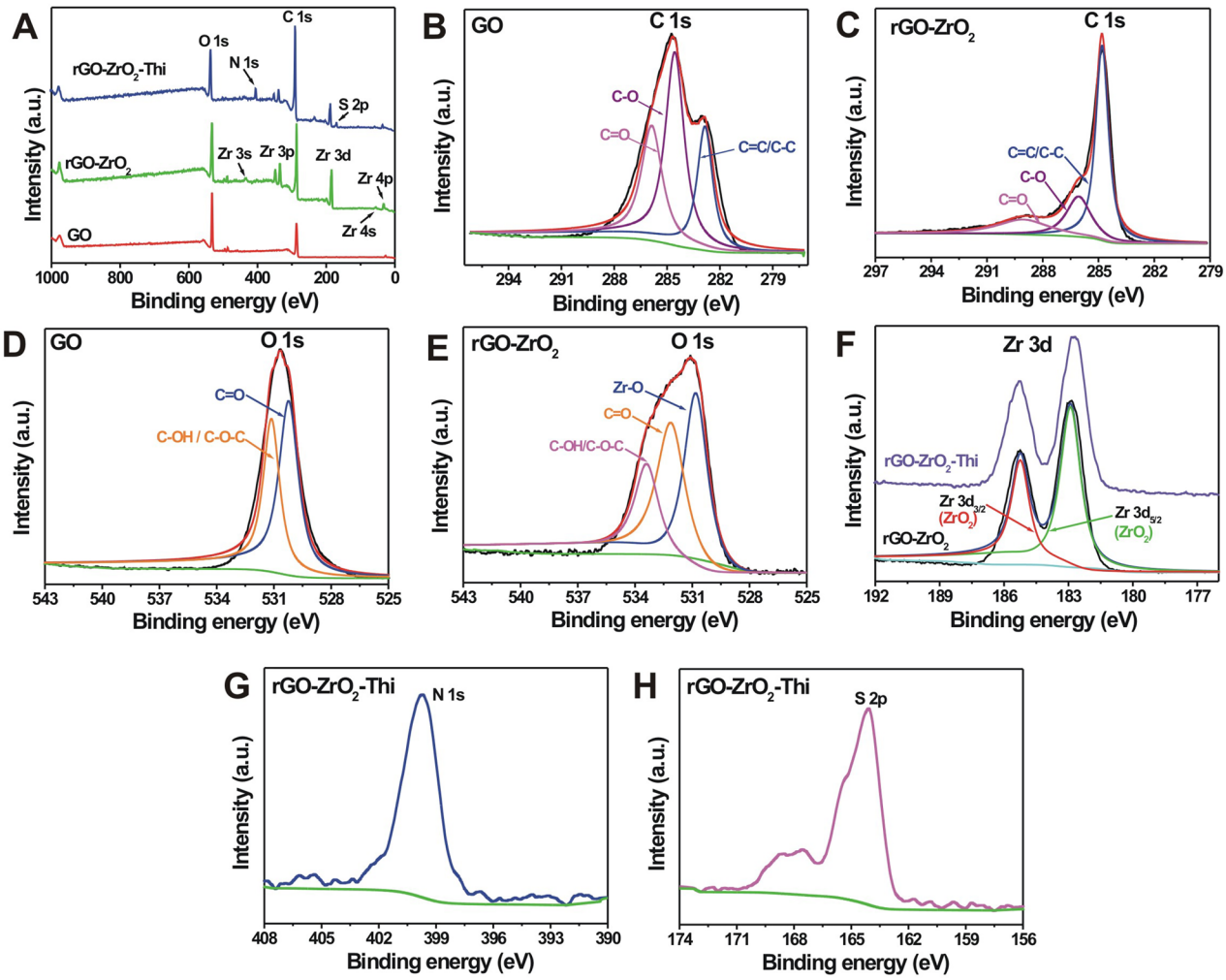

Figure 2. XPS survey spectra of GO, rGO-ZrO_2, and rGO-ZrO_2−Thi (A). The C 1s binding energy of GO (B) and rGO-ZrO_2 (C). The O 1s binding energy of GO (D) and rGO-ZrO_2 (E). The Zr 3d binding energy of the rGO-ZrO_2 and rGO-ZrO_2−Thi nanocomposites (F). The N 1s (G) and S 2p (H) binding energy of the rGO-ZrO_2−Thi nanocomposite.

and the phosphate group, generating an amplified electrochemical response toward PKA activity.

3.2. Experimental Characterization of GO, rGO-ZrO_2, and rGO-ZrO_2−Thi Nanocomposites. The morphology characterization toward GO and rGO-ZrO_2 was shown in Figure 1. The TEM image of GO appeared transparent and folded over the edges (Figure 1A). The ZrO_2 nanoparticles with the size mostly in the range 5−20 nm were grown onto the rGO surface (Figure 1B). A high-resolution TEM image revealed that the measured interplanar spacing of a single crystalline ZrO_2 nanoparticle was about 0.294 nm, which was consistent with the value of monoclinic ZrO_2 (Figure 1C). The corresponding SEM characterizations and photographs toward GO and rGO-ZrO_2 were also shown in Figure S1. The crystalline structures for GO and rGO-ZrO_2 were characterized by XRD methods and shown in Figure 1D. The GO showed a diffraction peak at 2θ = 10.8°, which corresponded to the (001) reflection of GO. Such a diffraction peak disappeared for rGO-ZrO_2, suggesting the successful reduction of GO into rGO. Also, other diffraction peaks related with ZrO_2 could conform well with the card (JCPDS no. 37-1484), indicating a monoclinic crystal phase of ZrO_2 on the rGO surface.[49] The successful synthesis of rGO-ZrO_2 nanomaterials was further characterized by FTIR spectra (Figure 1F). The corresponding absorption bands were listed in Table S1. The GO showed the characteristic peaks corresponding to the oxygen-containing groups. These peaks disappeared or decreased for rGO-ZrO_2, indicating again the successful reduction of GO into rGO during the hydrothermal treatment.[50] The new peaks located at about 742 and 590 cm^{-1} were due to the Zr−O stretching vibrations. The new broad peak at 1162 cm^{-1} might be attributed to the C−O−Zr bond, suggesting the chemical interaction of formed ZrO_2 with rGO.[44] The EDX spectra revealed the corresponding elements and contents of C, O, and Zr in GO and rGO-ZrO_2, respectively (Figure S2). Also, it could be seen from the elemental mapping images (C, Zr, and O) of rGO-ZrO_2 that the ZrO_2 nanoparticles were homogeneously distributed onto the rGO surface (Figure 1E). The thermogravimetric (TG) curves illustrated that rGO-ZrO_2 possessed a remarkable thermal stability compared to GO (Figure S3).

XPS is a powerful technique that can directly allow the analysis of elemental composition of the GO, rGO-ZrO_2, and rGO-ZrO_2−Thi nanocomposites. The full XPS scan for the GO, rGO-ZrO_2, and rGO-ZrO_2−Thi nanocomposites was shown in Figure 2A. An increase of C/O ratio from 1.91 (GO) to 2.73 (rGO-ZrO_2) indicated the decreased oxygen-containing groups after reduction. After thionine adsorption

DOI: 10.1021/acsabm.8b00451
ACS Appl. Bio Mater. XXXX, XXX, XXX−XXX

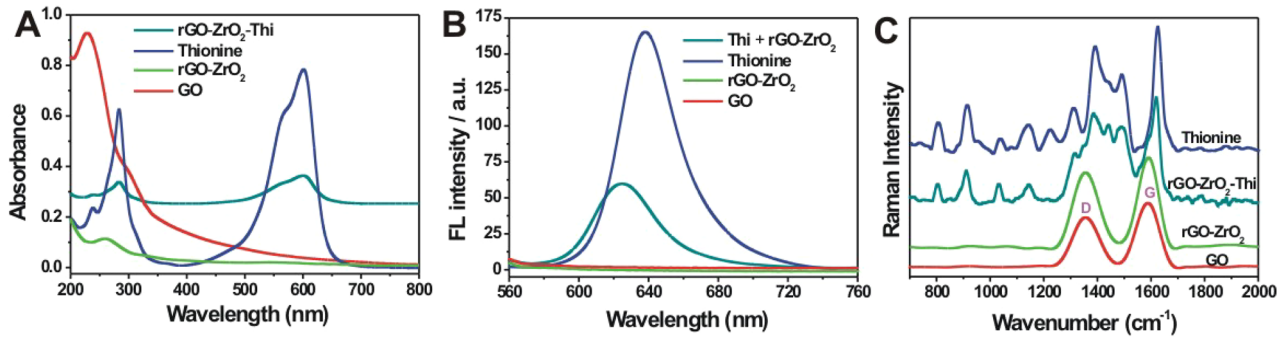

Figure 3. (A) UV−vis spectroscopy of GO (red), rGO-ZrO_2 (green), thionine (blue), and rGO-ZrO_2−Thi (dark cyan) in the aqueous solution, respectively. (B) Fluorescence spectroscopy for GO (red), rGO-ZrO_2 (green), and thionine before (blue) and after (dark cyan) the addition of rGO-ZrO_2. (C) Raman spectroscopy of GO (red), rGO-ZrO_2 (green), thionine (blue), and rGO-ZrO_2−Thi (dark cyan), respectively.

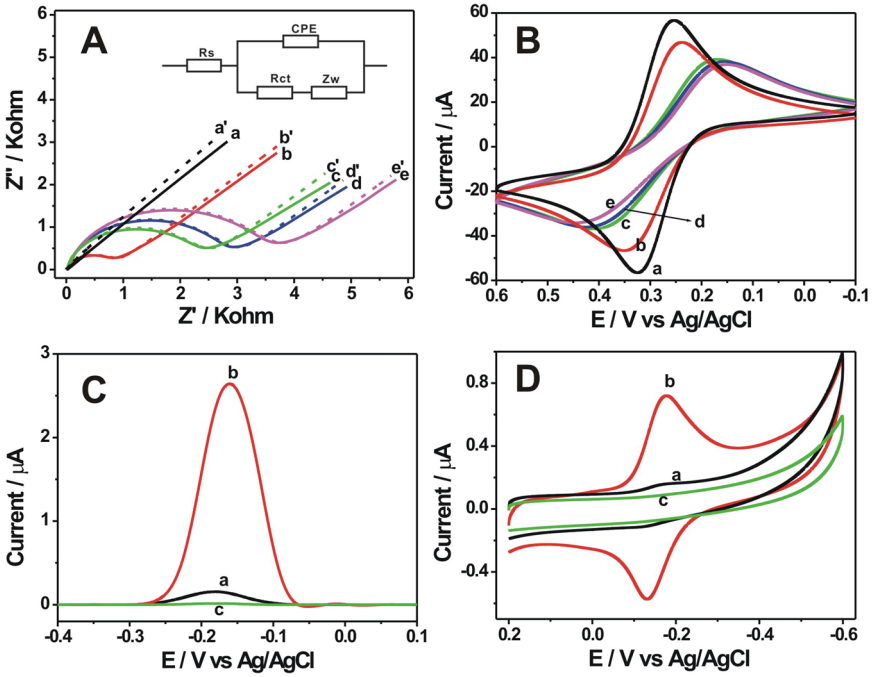

Figure 4. Electrochemical impedance spectroscopy (A) and cyclic voltammetry (B) for the differently assembled electrodes in 5 mM $[Fe(CN)_6]^{3-/4-}$ of 10 mM PBS buffer (pH 7.4, 1 M KCl) including the bare gold electrode (a), kemptide-immobilized electrode (b), after MCH blocking (c), phosphorylation of kemptide (d), and recognition with the rGO-ZrO_2−Thi nanocomposite (e). EIS was operated with the frequency range from 0.1 Hz to 10 kHz and the amplitude of 5 mV. The dashed (a′−e′) and solid lines (a−e) were for experimental and simulated EIS curves, respectively. The inset shows the corresponding equivalent circuit. The scan rates for CV were 100 mV/s. Differential pulse voltammetric (C) and cyclic voltammetric (D) responses of the fabricated PKA biosensor toward blank (a) and 20 U/mL PKA (b) in 10 mM PBS (pH 7.4). The curve (c) was obtained by using rGO-ZrO_2 as the substitute of the rGO-ZrO_2−Thi nanocomposite. The ATP concentration is 80 μM. The reaction time for PKA catalysis is 1.5 h.

onto the rGO-ZrO_2 surface, the C/O ratio was further increased to 3.93. The C 1s peaks for GO and rGO-ZrO_2 were split into three peaks corresponding to C═C/C—C, C—O, and C═O, respectively (Figure 2B,C), which were in basic accordance with the FTIR results. Also, in O 1s of rGO-ZrO_2, a peak at 530.8 eV corresponding to Zr−O appeared besides the peaks for C═O and C—O—C/C—OH (Figure 2D,E). It could be further seen that the binding energy of the C 1s and O 1s peaks of rGO-ZrO_2 increased compared with GO, suggesting the electron supply from Zr to C and O. The Zr 3d of rGO-ZrO_2 (Figure 2F) was split into Zr $3d_{5/2}$ (182.90 eV) and Zr $3d_{3/2}$ (185.24 eV), which was the typical characteristic for the Zr^{4+} ion in the full oxidation state.[42,49,51] After assembly of thionine on rGO-ZrO_2, the Zr $3d_{5/2}$ peak at 182.9 eV of rGO-ZrO_2 was shifted to 182.4 eV for rGO-ZrO_2−Thi, which could be attributed to the electrostatic attraction force between zirconium and thionine. It also confirmed the adsorption of thionine onto the rGO surface via $\pi-\pi$ stacking.[43] Also, as shown in Figure 2G,H, two new peaks centered at 164.1 and 399.7 eV correspond to the S 2p and N 1s of thionine, further revealing the existence of thionine on the rGO-ZrO_2 surface.

3.3. UV−Vis, Fluorescence, and Raman Spectroscopy Characterizations toward the rGO-ZrO_2−Thi Nanocomposite. The assembly of thionine onto the rGO-ZrO_2 surface was verified by UV−vis spectroscopy (Figure 3A). The GO displayed a typical absorption peak at 228 nm and a shoulder peak at 300 nm.[46,52] The maximum absorption of rGO-ZrO_2 shifted to be about 260 nm, suggesting the reduction of GO into rGO for the recovery of electronic conjugation. The thionine showed two characteristic peaks at

DOI: 10.1021/acsabm.8b00451
ACS Appl. Bio Mater. XXXX, XXX, XXX−XXX

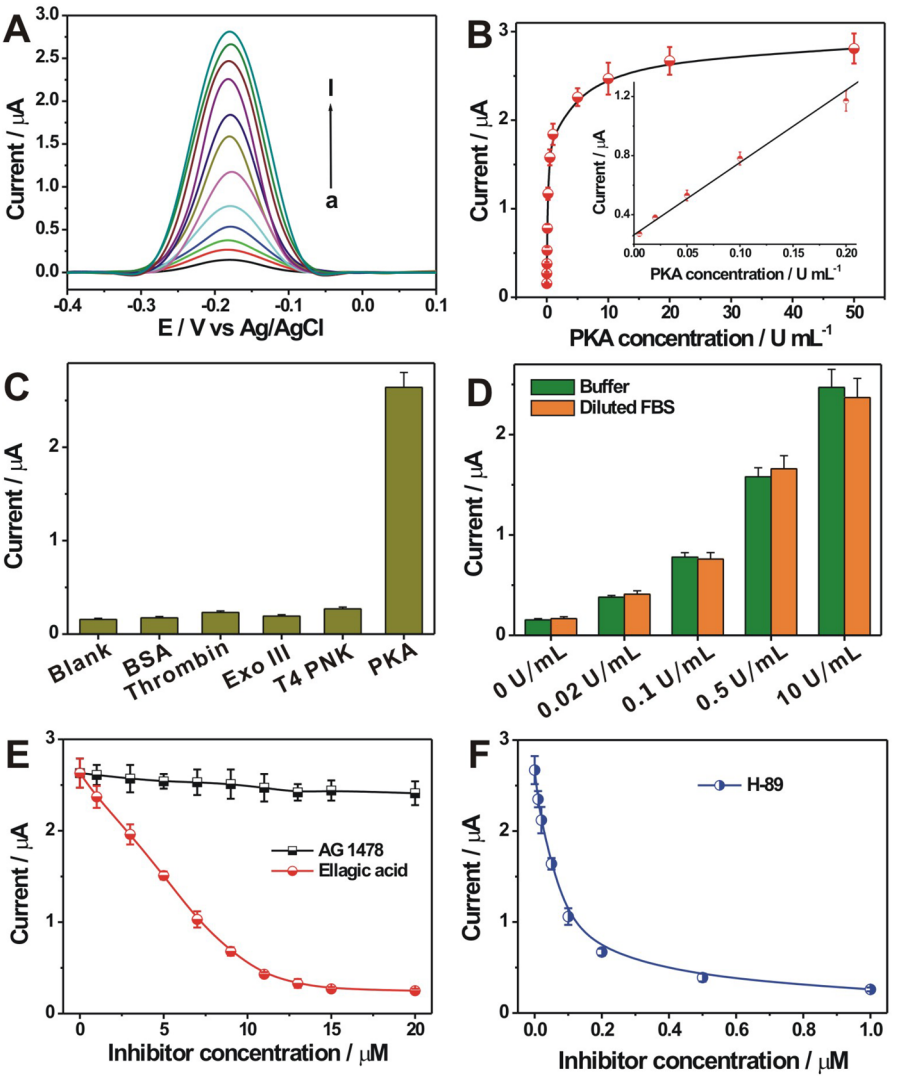

Figure 5. (A) DPV responses of the fabricated biosensor toward different concentrations of PKA. The concentrations for the curves (a–l) were 0, 0.005, 0.02, 0.05, 0.1, 0.2, 0.5, 1, 5, 10, 20, and 50 U/mL, respectively. (B) Calibration curve between DPV peak current and PKA concentration. The inset shows the linear relationship. (C) Selectivity test of the fabricated biosensor toward different proteins including bovine serum albumin (BSA, 1 μM), thrombin (1 μM), Exo III (20 U/mL), T4 PNK (20 U/mL), and PKA (20 U/mL). (D) Electrochemical responses in buffer and 5% diluted FBS spiked with different concentrations of PKA. (E) Relationship of DPV responses with ellagic acid and tyrphostin AG 1478 concentrations. The used concentrations for ellagic acid and tyrphostin AG 1478 were 1, 3, 5, 7, 9, 11, 13, 15, and 20 μM. (F) Relationship of DPV responses with H-89 concentrations. The used concentrations for H-89 were 10, 20, 50, 100, 200, 500, and 1000 nM, respectively. The PKA and ATP concentrations used in panels E and F were 20 U/mL and 80 μM, respectively.

about 283 and 600 nm, respectively,[53] which could be also observed in the obtained rGO-ZrO_2–Thi nanocomposites. The fluorescence experiment further evidenced the assembly of thionine onto the rGO-ZrO_2 surface (Figure 3B). It is well-known that graphene oxide can work as a quencher when it interacts with the fluorescent molecules. The thionine in the solution displayed a fluorescence emission at 638 nm. The fluorescence intensity evidently decreased after addition of rGO-ZrO_2, suggesting an interaction between thionine and rGO-ZrO_2. Raman spectroscopy characterizations were shown in Figure 3C. Two characteristic peaks at 1355 and 1589 cm^{-1} corresponding to D and G bands of carbon atoms were observed in GO and rGO-ZrO_2.[54] The typical peaks of thionine (807, 912, and 1389 cm^{-1}) were also seen in the spectrum of the rGO-ZrO_2–Thi nanocomposite, which could be attributed to the atom vibration of thionine rings.[55] These experiments fully evidenced the assembly of thionine onto rGO-ZrO_2 to form a rGO-ZrO_2–Thi nanocomposite.

3.4. Electrochemical Characterization of the Biosensor Fabrication Process and Detection Feasibility toward PKA. The stepwise assembly processes for PKA biosensor fabrication were followed by electrochemical impedance spectroscopy (EIS) methods (Figure 4A). The inset showed the corresponding equivalent circuit. The experimental curves for differently modified electrodes (dashed lines from a′ to e′) agreed well with the simulated curves (solid lines from a to e). The obtained parameters by fitting Nyquist plots were shown in Table S2. A straight curve was observed for the bare electrode, indicating a diffusion-controlled electrochemical process (curves a and a′). After kemptide and MCH assembly on the electrode, the charge transfer resistance (Rct) was increased sequentially with the obtained values of 1032 Ω (curves b and b′) and 2481 Ω (curves c and

DOI: 10.1021/acsabm.8b00451
ACS Appl. Bio Mater. XXXX, XXX, XXX–XXX

c′), suggesting the inhibition effect of immobilized insulating molecules on the $[Fe(CN)_6]^{3-/4-}$ diffusion. After kemptide phosphorylation catalyzed by PKA, the electrochemical impedance increased slightly to 2815 Ω, which might be due to the introduced negative charge after kemptide phosphorylation (curves d and d′). After the binding of rGO-ZrO_2−Thi on the electrode via the multicoordinative interaction of ZrO_2 with the phosphate group, the impedance was observed with a further increase (3512 Ω) (curves e and e′). Although rGO has been well-known to improve the electron transfer ability, the observed phenomenon of the increased Rct value might be induced by the anchored ZrO_2 with the increased negative charges. The corresponding cyclic voltammetric characterizations for the differently modified electrodes were shown in Figure 4B. The nearly reversible redox peaks of $[Fe(CN)_6]^{3-/4-}$ could be seen on the bare electrode surface (curve a). Following a stepwise assembly of the biosensor fabrication process, the peak current decreased and the peak-to-peak potential (ΔE_p) increased sequentially (curves b to e), indicating the suppressive $[Fe(CN)_6]^{3-/4-}$ diffusion for the decreased electrochemical response after a stepwise assembly process. The cyclic voltammetric responses for the differently assembled electrodes were basically in accordance with the EIS results, indicating the successful fabrication of an electrochemical biosensor.

The detection feasibility toward PKA activity was then confirmed and shown in Figure 4C,D. An evidently amplified DPV response related with the electrochemical reduction of thionine at about −0.16 V could be observed after kemptide phosphorylation by PKA and binding with the rGO-ZrO_2−Thi nanocomposite (curve b in Figure 4C). Also, a pair of large redox peaks of thionine could be seen in the CV results (curve b in Figure 4D). The linear relationship between peak currents and scan rates indicated the surface-controlled electrochemical redox process (data not shown). The electrochemical response was only very small when no PKA was applied (curve a in Figure 4C,D), suggesting that no phosphate group was introduced in the kemptide and that the rGO-ZrO_2−Thi could not effectively bind on the electrode surface. Furthermore, we used rGO-ZrO_2 with no thionine assembly as a comparison. No electrochemical responses could be obtained (curve c in Figure 4C,D). These experiments fully evidenced the electrochemical detection feasibility toward PKA activity. The signal-to-background (S/B) value for the detection of 20 U/mL PKA could reach an exciting value of about 20. It should be noted that, in the case of detection toward different types of protein kinases, especially with negatively charged kemptide substrate, the nonspecific electrostatic interaction between the rGO-ZrO_2−Thi nanocomposite and kemptide might exist for a relatively high background signal. However, the multicoordinative interaction between ZrO_2 and the phosphate group would dominate. Also, the nonspecific electrostatic interaction between the rGO-ZrO_2−Thi nanocomposite and kemptide might be decreased to some extent by changing the solution pH or even the kemptide sequence. Thus, the current rGO-ZrO_2−Thi nanocomposite has the potential for the generic detection of different protein kinases.

3.5. Experimental Condition Optimization. The experimental optimization was performed to pursue the best detection performance (Figure S4). The immobilization concentration of kemptide was first determined as 200 μM, superior to other employed concentrations (Figure S4A). The loading amount of ZrO_2 onto the surface of rGO would impact the detection toward PKA activity. Too much of ZrO_2 decorated onto the rGO surface would be not beneficial for the further assembly of thionine onto the nanocomposite, but a low amount of ZrO_2 might limit the recognition of nanocomposite for the phosphorylated kemptide. Our experimental results showed that the rGO-ZrO_2−Thi nanocomposite prepared by GO and $ZrOCl_2$ with a mass ratio of 1:1 was superior to that by other mass ratios (Figure S4B). The thionine concentration for the preparation of the rGO-ZrO_2−Thi nanocomposite was also optimized. It could be seen that the rGO-ZrO_2−Thi nanocomposite prepared by 1 mM thionine could almost achieve the maximum response toward PKA activity detection, suggesting the saturation adsorption of thionine onto the rGO surface (Figure S4C). Furthermore, the ATP concentration, PKA catalysis time, and temperature were optimized as 80 μM, 90 min, and 37 °C, respectively (Figure S4D−F).

3.6. Detection Performance of the Fabricated Biosensor toward PKA Activity. The sensing performance toward PKA activity was further explored and shown in Figure 5A. A stepwise increase of the DPV response could be seen upon the addition of increasing PKA concentration (0−50 U/mL), indicating a concentration-dependent response manner. The calibration curve for the peak current versus PKA concentration was obtained (Figure 5B). A linear plot as Y (peak current, μA) = 0.26 + 4.90 X (concentration, U/mL) was demonstrated in the PKA concentration range 0.005−0.2 U/mL (correlative coefficient, 0.9921). The detection limit toward PKA could be experimentally achieved as 0.005 U/mL, which was evidently lower than the vast majority of reported methods (Table S3). Thus, the fabricated PKA biosensor could achieve the ultrasensitive detection toward PKA activity. Six repetitive measurements toward three concentrations of PKA (0.5, 1, and 20 U/mL) displayed the relative standard deviations (RSDs) of 6.79%, 7.3%, and 5.8%, respectively. Thus, the detection reproducibility of the current biosensor for PKA is satisfied.

The selectivity test of the current biosensor toward several different proteins was also conducted (Figure 5C). Only a distinct electrochemical response toward PKA could be obtained when compared with other nonspecific proteins. Also, we attempted the PKA detection in the diluted serum samples by the current biosensor to verify its applicative potential in a relatively complex biological matrix (Figure 5D). The blank serum could only give a slightly larger electrochemical response than the blank buffer, suggesting that the diluted serum itself contained no or only a very little amount of PKA, which could be not discriminated by the current biosensor. Also, the current responses in the serum toward PKA were comparable with that in the buffer and intensified with the increasing concentrations of spiked PKA. This strongly suggested the applicative potential in the complex biological sample.

3.7. Inhibitor Screening of the Current PKA Biosensor. The developed electrochemical biosensor was further explored for PKA inhibitor screening. Herein, ellagic acid and H-89 were chosen since they had been well-recognized as efficient PKA inhibitors. The DPV response could be effectively inhibited whether for the addition of ellagic acid or H-89 (Figure 5E,F). The IC_{50} values of ellagic acid and H-89 were obtained as 5.36 μM and 67 nM, which were basically consistent with the reported values.[25,30,56,57] Also, a tyrosine

DOI: 10.1021/acsabm.8b00451
ACS Appl. Bio Mater. XXXX, XXX, XXX−XXX

kinase inhibitor (tyrphostin AG 1478) was used to check its effect on PKA activity. In this case, only a negligible DPV peak current change could be observed upon addition of an increasing tyrphostin AG 1478 concentration, suggesting no inhibition effect on PKA activity. These experiments showed the potential of the current fabricated biosensor in the PKA inhibitor screening.

4. CONCLUSION

In the current study, a novel rGO-ZrO_2−Thi nanocomposite was successfully prepared and directly used for label-free electrochemical analysis of PKA activity. The rGO-ZrO_2−Thi nanocomposite was well-characterized by various techniques. It took full advantage of the specific recognition of ZrO_2 nanoparticles for the phosphate group, the abundant thionines attached onto the rGO surface for signal amplification and transduction, as well as unique electronic properties of rGO. The fabricated PKA biosensor by the rGO-ZrO_2−Thi nanocomposite could effectively avoid the expensive or specialized assay reagents or complex post-treatment procedures for many existing PKA assay methods. The detection limit toward PKA could be achieved as 0.005 U/mL. Also, it could be efficiently applied for inhibitor screening. Therefore, the currently fabricated biosensor could be used as a generic and sensitive strategy for the protein kinase activity assay to serve for disease diagnosis, prognosis, and drug discovery.

■ ASSOCIATED CONTENT

Supporting Information

The Supporting Information is available free of charge on the ACS Publications website at DOI: 10.1021/acsabm.8b00451.

SEM, EDX, and thermal gravity (TG) characterizations toward GO and rGO-ZrO_2; corresponding bands for FTIR and parameters by fitting Nyquist plots; PKA assay condition optimization; PKA performance comparison (PDF)

■ AUTHOR INFORMATION

Corresponding Author

*E-mail: sliu@qust.edu.cn. Tel: 86-532-84022681.

ORCID

Shufeng Liu: 0000-0003-4063-4537

Notes

The authors declare no competing financial interest.

■ ACKNOWLEDGMENTS

We appreciate the financial support from the National Natural Science Foundation of China (21475072), the Natural Science Foundation of Shandong Province of China (JQ201704 and ZR2015JL007), the Key Research and Development Program of Shandong Province of China (2016GSF201208), and the Open Project from Fujian Provincial Key Laboratory of Ecology-Toxicological Effects & Control for Emerging Contaminants.

■ REFERENCES

(1) Manning, G.; Whyte, D. B.; Martinez, R.; Hunter, T.; Sudarsanam, S. The Protein Kinase Complement of the Human Genome. *Science* **2002**, *298*, 1912−1934.

(2) Hunter, T. Signaling-2000 and Beyond. *Cell* **2000**, *100*, 113−127.

(3) Kahn, B. B.; Alquier, T.; Carling, D.; Hardie, D. G. AMP-Activated Protein Kinase: Ancient Energy Gauge Provides Clues to Modern Understanding of Metabolism. *Cell Metab.* **2005**, *1*, 15−25.

(4) Hardie, D. G. AMP-Activated Protein Kinase: a Key Regulator of Energy Balance with Many Roles in Human Disease. *J. Int. Med.* **2014**, *276*, 543−559.

(5) Skorski, T. Oncogenic Tyrosine Kinases and the DNA-Damage Response. *Nat. Rev. Cancer* **2002**, *2*, 351−360.

(6) Salminen, A.; Kaarniranta, K.; Haapasalo, A.; Soininen, H.; Hiltunen, M. AMP-Activated Protein Kinase: a Potential Player in Alzheimer's Disease. *J. Neurochem.* **2011**, *118*, 460−474.

(7) Noble, M. E. M.; Endicott, J. A.; Johnson, L. N. Protein Kinase Inhibitors: Insights into Drug Design from Structure. *Science* **2004**, *303*, 1800−1805.

(8) Cohen, P.; Alessi, D. R. Kinase Drug Discovery-What's Next in the Field? *ACS Chem. Biol.* **2013**, *8*, 96−104.

(9) Houseman, B. T.; Huh, J. H.; Kron, S. J.; Mrksich, M. Peptide Chips for the Quantitative Evaluation of Protein Kinase Activity. *Nat. Biotechnol.* **2002**, *20*, 270−274.

(10) Shults, M. D.; Imperiali, B. Versatile Fluorescence Probes of Protein Kinase Activity. *J. Am. Chem. Soc.* **2003**, *125*, 14248−14249.

(11) Li, X.; Zhu, L.; Zhou, Y.; Yin, H.; Ai, S. Enhanced Photoelectrochemical Method for Sensitive Detection of Protein Kinase A Activity Using TiO2/gC3N4, PAMAM Dendrimer, and Alkaline Phosphatase. *Anal. Chem.* **2017**, *89*, 2369−2376.

(12) Xu, X.; Liu, X.; Nie, Z.; Pan, Y.; Guo, M.; Yao, S. Label-Free Fluorescent Detection of Protein Kinase Activity Based on the Aggregation Behavior of Unmodified Quantum Dots. *Anal. Chem.* **2011**, *83*, 52−59.

(13) Herbst, K. J.; Allen, M. D.; Zhang, J. Luminescent Kinase Activity Biosensors Based on a Versatile Bimolecular Switch. *J. Am. Chem. Soc.* **2011**, *133*, 5676−5679.

(14) Zhang, L.; Song, W.; Liang, R. P.; Qiu, J. D. Simultaneous Determination of Protein Kinase A and Casein Kinase II by Dual-Color Peptide Biomineralized Metal Nanoclusters. *Anal. Chem.* **2016**, *88*, 11460−11467.

(15) Min, D. H.; Su, J.; Mrksich, M. Profiling Kinase Activities by Using a Peptide Chip and Mass Spectrometry. *Angew. Chem., Int. Ed.* **2004**, *43*, 5973−5977.

(16) Liu, J.; Cheng, H.; He, D.; He, X.; Wang, K.; Liu, Q.; Zhao, S.; Yang, X. Label-Free Homogeneous Electrochemical Sensing Platform for Protein Kinase Assay Based on Carboxypeptidase Y-Assisted Peptide Cleavage and Vertically Ordered Mesoporous Silica Films. *Anal. Chem.* **2017**, *89*, 9062−9068.

(17) He, S.; Kyaw, Y. M. E.; Tan, E. K. M.; Bekale, L.; Kang, M. W. C.; Kim, S. S. Y.; Tan, I.; Lam, K. P.; Kah, J. C. Y. Quantitative and Label-Free Detection of Protein Kinase A Activity Based on Surface-Enhanced Raman Spectroscopy with Gold Nanostars. *Anal. Chem.* **2018**, *90*, 6071−6080.

(18) Liu, X.; Dong, M.; Qi, H.; Gao, Q.; Zhang, C. Electrogenerated Chemiluminescence Bioassay of Two Protein Kinases Incorporating Peptide Phosphorylation and Versatile Probe. *Anal. Chem.* **2016**, *88*, 8720−8727.

(19) Wang, Z.; Lévy, R.; Fernig, D. G.; Brust, M. Kinase-Catalyzed Modification of Gold Nanoparticles: a New Approach to Colorimetric Kinase Activity Screening. *J. Am. Chem. Soc.* **2006**, *128*, 2214−2215.

(20) Kerman, K.; Song, H.; Duncan, J. S.; Litchfield, D. W.; Kraatz, H. B. Peptide Biosensors for the Electrochemical Measurement of Protein Kinase Activity. *Anal. Chem.* **2008**, *80*, 9395−9401.

(21) Xu, S.; Liu, Y.; Wang, T.; Li, J. Highly Sensitive Electrogenerated Chemiluminescence Biosensor in Profiling Protein Kinase Activity and Inhibition Using Gold Nanoparticle as Signal Transduction Probes. *Anal. Chem.* **2010**, *82*, 9566−9572.

(22) Gu, C.; Gai, P.; Han, L.; Yu, W.; Liu, Q.; Li, F. Enzymatic Biofuel Bell-Based Self-Powered Biosensing of Protein Kinase Activity and Inhibition via Thiophosphorylation-Mediated Interface Engineering. *Chem. Commun.* **2018**, *54*, 5438−5441.

(23) Freeman, R.; Finder, T.; Gill, R.; Willner, I. Probing Protein Kinase (CK2) and Alkaline Phosphatase with CdSe/ZnS Quantum Dots. *Nano Lett.* **2010**, *10*, 2192−2196.
(24) Martic, S.; Labib, M.; Freeman, D.; Kraatz, H. B. Probing the Role of the Linker in Ferrocene−ATP Conjugates: Monitoring Protein Kinase Catalyzed Phosphorylations Electrochemically. *Chem. - Eur. J.* **2011**, *17*, 6744−6752.
(25) Wang, L. J.; Yang, Y.; Zhang, C. Y. Phosphorylation-Directed Assembly of a Single Quantum Dot Based Nanosensor for Protein Kinase Assay. *Anal. Chem.* **2015**, *87*, 4696−4703.
(26) Li, T.; Liu, X.; Liu, D.; Wang, Z. Sensitive Detection of Protein Kinase A Activity in Cell Lysates by Peptide Microarray-Based Assay. *Anal. Chem.* **2013**, *85*, 7033−7037.
(27) Zhou, Y.; Wang, M.; Yang, Z.; Yin, H.; Ai, S. A Phos-Tag-Based Photoelectrochemical Biosensor for Assay of Protein Kinase Activity and Inhibitors. *Sens. Actuators, B* **2015**, *206*, 728−734.
(28) Liu, C.; Chang, L.; Wang, H.; Bai, J.; Ren, W.; Li, Z. Upconversion Nanophosphor: An Efficient Phosphopeptides-Recognizing Matrix and Luminescence Resonance Energy Transfer Donor for Robust Detection of Protein Kinase Activity. *Anal. Chem.* **2014**, *86*, 6095−6102.
(29) Lowe, S. B.; Dick, J. A. G.; Cohen, B. E.; Stevens, M. M. Multiplex Sensing of Protease and Kinase Enzyme Activity via Orthogonal Coupling of Quantum Dot−Peptide Conjugates. *ACS Nano* **2012**, *6*, 851−857.
(30) Ji, J.; Yang, H.; Liu, Y.; Chen, H.; Kong, J.; Liu, B. TiO_2-Assisted Silver Enhanced Biosensor for Kinase Activity Profiling. *Chem. Commun.* **2009**, 1508−1510.
(31) Wang, J.; Cao, Y.; Li, Y.; Liang, Z.; Li, G. Electrochemical Strategy for Detection of Phosphorylation Based on Enzyme-Linked Electrocatalysis. *J. Electroanal. Chem.* **2011**, *656*, 274−278.
(32) Zhang, X.; Liu, C.; Wang, H.; Wang, H.; Li, Z. Rare Earth Ion Mediated Fluorescence Accumulation on a Single Microbead: An Ultrasensitive Strategy for the Detection of Protein Kinase Activity at the Single-Cell Level. *Angew. Chem., Int. Ed.* **2015**, *54*, 15186−15190.
(33) Ren, W.; Liu, C.; Lian, S.; Li, Z. Flow Cytometry-Assisted Mix-and-Read Assay for Ultrasensitive Detection of Protein Kinase Activity by use of Zr^{4+}-Functionalized Mesoporous SiO_2 Microspheres. *Anal. Chem.* **2013**, *85*, 10956−10961.
(34) Monot, J.; Petit, M.; Lane, S. M.; Guisle, I.; Léger, J.; Tellier, C.; Talham, D. R.; Bujoli, B. Towards Zirconium Phosphonate-Based Microarrays for Probing DNA−Protein Interactions: Critical Influence of the Location of the Probe Anchoring Groups. *J. Am. Chem. Soc.* **2008**, *130*, 6243−6251.
(35) Pang, H.; Lu, Q.; Gao, F. Graphene Oxide Induced Growth of One-Dimensional Fusiform Zirconia Nanostructures for Highly Selective Capture of Phosphopeptides. *Chem. Commun.* **2011**, *47*, 11772−11774.
(36) Yan, Z.; Wang, Z.; Miao, Z.; Liu, Y. Dye-Sensitized and Localized Surface Plasmon Resonance Enhanced Visible-Light Photoelectrochemical Biosensors for Highly Sensitive Analysis of Protein Kinase Activity. *Anal. Chem.* **2016**, *88*, 922−929.
(37) Miao, P.; Ning, L.; Li, X.; Li, P.; Li, G. Electrochemical Strategy for Sensing Protein Phosphorylation. *Bioconjugate Chem.* **2012**, *23*, 141−145.
(38) Wang, Z.; Sun, N.; He, Y.; Liu, Y.; Li, J. DNA Assembled Gold Nanoparticles Polymeric Network Blocks Modular Highly Sensitive Electrochemical Biosensors for Protein Kinase Activity Analysis and Inhibition. *Anal. Chem.* **2014**, *86*, 6153−6159.
(39) Xu, X.; Nie, Z.; Chen, J.; Fu, Y.; Li, W.; Shen, Q.; Yao, S. A DNA-Based Electrochemical Strategy for Label-Free Monitoring the Activity and Inhibition of Protein Kinase. *Chem. Commun.* **2009**, 6946−6948.
(40) Hu, Q.; Wang, Q.; Jiang, C.; Zhang, J.; Kong, J.; Zhang, X. Electrochemically Mediated Polymerization for Highly Sensitive Detection of Protein Kinase Activity. *Biosens. Bioelectron.* **2018**, *110*, 52−57.
(41) Zhang, G. Y.; Cai, C.; Cosnier, S.; Zeng, H. B.; Zhang, X. J.; Shan, D. Zirconium-Metalloporphyrin Frameworks as a Three-in-One Platform Possessing Oxygen Nanocage, Electron Media, and Bonding Site for Electrochemiluminescence Protein Kinase Activity Assay. *Nanoscale* **2016**, *8*, 11649−11657.
(42) Luo, X.; Wang, X.; Bao, S.; Liu, X.; Zhang, W.; Fang, T. Adsorption of Phosphate in Water Using One-Step Synthesized Zirconium-Loaded Reduced Graphene Oxide. *Sci. Rep.* **2016**, *6*, 39108.
(43) Giri, S.; Ghosh, D.; Das, C. K. Growth of Vertically Aligned Tunable Polyaniline on Graphene/ZrO_2 Nanocomposites for Supercapacitor Energy-Storage Application. *Adv. Funct. Mater.* **2014**, *24*, 1312−1324.
(44) Zhou, Q.; Huang, J.; Wang, J.; Yang, Z.; Liu, S.; Wang, Z.; Yang, S. Preparation of a Reduced Graphene Oxide/Zirconia Nanocomposite and its Application as a Novel Lubricant Oil Additive. *RSC Adv.* **2015**, *5*, 91802−91812.
(45) Li, W.; Wu, P.; Zhang, H.; Cai, C. Signal Amplification of Graphene Oxide Combining with Restriction Endonuclease for Site-Specific Determination of DNA Methylation and Assay of Methyltransferase Activity. *Anal. Chem.* **2012**, *84*, 7583−7590.
(46) Zhou, Q.; Li, G.; Zhang, Y.; Zhu, M.; Wan, Y.; Shen, Y. Highly Selective and Sensitive Electrochemical Immunoassay of Cry1C Using Nanobody and $\pi-\pi$ Stacked Graphene Oxide/Thionine Assembly. *Anal. Chem.* **2016**, *88*, 9830−9836.
(47) Liu, S.; Fang, L.; Wang, Y.; Wang, L. Universal Dynamic DNA Assembly-Programmed Surface Hybridization Effect for Single-Step, Reusable, and Amplified Electrochemical Nucleic Acid Biosensing. *Anal. Chem.* **2017**, *89*, 3108−3115.
(48) Lu, J.; Zang, J. B.; Shan, S. X.; Huang, H.; Wang, Y. H. Synthesis and Characterization of Core-Shell Structural MWNT-Zirconia Nanocomposites. *Nano Lett.* **2008**, *8*, 4070−4074.
(49) Kumar, S.; Kumar, S.; Tiwari, S.; Srivastava, S.; Srivastava, M.; Yadav, B. K.; Kumar, S.; Tran, T. T.; Dewan, A. K.; Mulchandani, A.; Sharma, J. G.; Maji, S.; Malhotra, B. D. Biofunctionalized Nanostructured Zirconia for Biomedical Application: a Smart Approach for Oral Cancer Detection. *Adv. Sci.* **2015**, *2*, 1500048.
(50) Acik, M.; Lee, G.; Mattevi, C.; Pirkle, A.; Wallace, R. M.; Chhowalla, M.; Cho, K.; Chabal, Y. The Role of Oxygen during Thermal Reduction of Graphene Oxide Studied by Infrared Absorption Spectroscopy. *J. Phys. Chem. C* **2011**, *115*, 19761−19781.
(51) Shan, Y.; Gao, L. Synthesis and Characterization of Phase Controllable ZrO_2-Carbon Nanotube Nanocomposites. *Nanotechnology* **2005**, *16*, 625−630.
(52) Cui, D.; Mi, L.; Xu, X.; Lu, J.; Qian, J.; Liu, S. Nanocomposites of Graphene and Cytochrome P450 2D6 Isozyme for Electrochemical-Driven Tramadol Metabolism. *Langmuir* **2014**, *30*, 11833−11840.
(53) Ye, Y.; Xie, J.; Ye, Y.; Cao, X.; Zheng, H.; Xu, X.; Zhang, Q. A Label-Free Electrochemical DNA Biosensor Based on Thionine Functionalized Reduced Graphene Oxide. *Carbon* **2018**, *129*, 730−737.
(54) Zhu, Z.; Ma, L.; Su, M.; Liu, D.; Wang, Z. Preparation and Application of Thionin-Bridged Graphene-Gold Nanoparticle Nanohybrids. *J. Mater. Chem. B* **2013**, *1*, 1432−1438.
(55) Miotto, R.; Cunha, J. F. R.; Silva, S. W. d.; Soler, M. A. G.; Morais, P. C.; Ferraz, A. C.; Tada, D. B.; Petri, D. F. S.; Baptista, M. S. Thionin Adsorption on Silicon (1 0 0): Structural Analysis. *Appl. Surf. Sci.* **2006**, *253*, 1978−1982.
(56) Zhao, Z.; Zhou, X.; Xing, D. Highly Sensitive Protein Kinase Activity Assay Based on Electrochemiluminescence Nanoprobes. *Biosens. Bioelectron.* **2012**, *31*, 299−304.
(57) MacConaghy, K. I.; Geary, C. I.; Kaar, J. L.; Stoykovich, M. P. Photonic Crystal Kinase Biosensor. *J. Am. Chem. Soc.* **2014**, *136*, 6896−6899.

DOI: 10.1021/acsabm.8b00451
ACS Appl. Bio Mater. XXXX, XXX, XXX−XXX